

# Electronic properties of a graphene antidot in magnetic fields

P.S. Park<sup>1</sup>, S.C. Kim<sup>1</sup>, and S.-R. Eric Yang<sup>1,2\*</sup>

<sup>1</sup>Physics Department, Korea University, Seoul Korea

<sup>2</sup>Korea Institute for Advanced Study, Seoul Korea

(Dated: April 9, 2018)

We report on several unusual properties of a graphene antidot created by a piecewise constant potential in a magnetic field. We find that the total probability of finding the electron in the barrier can be nearly one while it is almost zero outside the barrier. In addition, for each electron state of a graphene antidot there is a dot state with exactly the same wavefunction but with a different energy. This symmetry is a consequence of Klein tunneling of Dirac electrons. Moreover, in zigzag nanoribbons we find strong coupling between some antidot states and zigzag edge states. Experimental tests of these effects are proposed.

PACS numbers:

## I. INTRODUCTION

Bulk Landau energy levels of graphene,  $E_n = \pm E_c \sqrt{2|n|}$ , have different magnetic field  $B$  and quantum number  $n$  dependence than those of ordinary two-dimensional Landau levels,  $E_n = \hbar\omega_c(n + 1/2)$  (Here the cyclotron energy  $\hbar\omega_c \propto B$ , where  $B$  is the magnetic field. The characteristic energy of Dirac electrons  $E_c \propto \sqrt{B}$ ). The wavefunctions of these two systems have, respectively, two-component and one-component structures[1]. In the presence of a dot or antidot potential these states of the two systems will be perturbed rather differently.

Electron wavefunctions of a graphene quantum dot have been investigated actively both with and without a magnetic field[2–12]: In absence of a magnetic field an electron cannot be localized due to Klein tunneling and only quasibound states are allowed. However, a perpendicular magnetic field enhances the localization of the wavefunctions and both bound states and quasibound states occur.

Recently properties of antidot lattices[13–19] have been explored actively. But properties of a single antidot in a magnetic field has not been studied thoroughly yet. We believe that an antidot created by cutting a hole out of the graphene sheet[13, 16] and an antidot induced by an electrostatic gate can have different properties. In an antidot created by holes skipping orbits that encircle an integer number of elementary quantum flux defined by the antidot are allowed[20]:  $BA \sim m\phi_0$ , where  $A$  is the enclosing area of the antidot,  $m$  is the orbital quantum number and  $\phi_0$  is the magnetic flux quantum. However, some graphene states of a gate induced antidot potential may not obey this quantization rule since Klein tunneling allows significant penetration into the barrier. Hence, graphene antidots may not always support skipping orbits at the edge of an antidot. Also we expect an antidot defined by a piecewise constant potential may have sev-

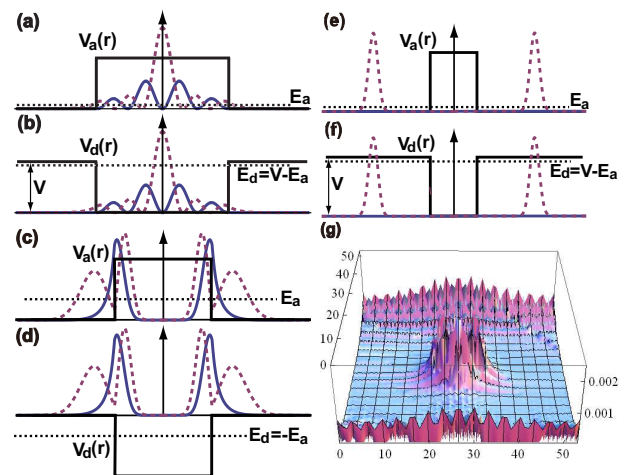


FIG. 1: Schematic drawings of some typical probability wavefunctions of antidots and dots. We consider piecewise constant antidot and dot potentials  $V_a(r)$  and  $V_d(r)$  satisfying  $V_a(r) + V_d(r) = V$ . (a) and (b) display dot and antidot states with the same wavefunction but with different energies  $E_d = V - E_a$  and  $E_a$ . Solid (dashed) line represents the probability wavefunction of A (B) component. Naively one may expect that the energy of the antidot state of (a) should be larger than the dot state by amount  $V$  since the antidot state is in the barrier with the height  $V$ , but this reasoning is actually incorrect. (c) and (d) are same as in (a) and (b) but with  $V_a(r) + V_d(r) = 0$ . Antidot and dot states have energies are  $E_a$  and  $E_d = -E_a$ . (e) and (f) are same as (a) and (b) but wavefunctions are localized outside the antidot and dot regions. (g) shows tight-binding probability wavefunction of an antidot state of a zigzag nanoribbon.

eral interesting properties in the presence of a magnetic field. This is because of the following feature of the Dirac equation: eigenstate wavefunctions of the Dirac equation are also eigenstates of Schrödinger-like equation, where constant potentials  $V$  and eigenvalue  $E$  appear together in the effective energy as  $E_{\text{eff}}^2 = (E - V)^2$ . This is an interesting feature of Dirac electrons but its consequences

\*corresponding author, eyang@venus.korea.ac.kr

have not been fully explored in a magnetic field. Nature of antidot states of a nanoribbon with zigzag edges may also be interesting. A nanoribbon has surface edges with various localization lengths[21, 22]. It is unclear whether these chiral zigzag edge states may be coupled to confined non-chiral antidot states.

In this paper we report on our investigation of these issues. We consider cylindrically symmetric and piecewise constant antidot potentials. We find that for each electron state of a graphene antidot there is a dot state with exactly the same wavefunction but with a different energy, see Figs.1(a)-(f). This symmetry is a consequence of the appearance of  $E_{\text{eff}}^2$  in the Schrödinger-like equation. We find that the eigenstates may be divided into three classes: those that are localized inside the antidot(Fig.1(a)), those that have significant weights at the boundary(Fig.1(c)), and those that are localized outside(Fig.1(e)). Interestingly we find that probability of finding the electron in the classically forbidden region of the *barrier* can be almost one, as shown in Figs.1(a) and (f). It is a counter example to the usual expectation that the probability wavefunction is larger in a potential well than in a barrier. This is a consequence of an interplay between strong Klein tunneling and localization of Landau level wavefunctions. In zigzag nanoribbons we find strong coupling between some antidot states and zigzag edge states, see Fig.1(g). This effect is unique to antidots of zigzag nanoribbons. Experimental tests of these effects are proposed.

## II. SYMMETRY BETWEEN ANTIDOT AND DOT STATES:

We consider a cylindrically symmetric and piecewise constant potential of an antidot or dot: where the radius of the antidot and dot is  $R$ :  $V(r) = V_{\text{I}}$  for  $r < R$  and  $V(r) = V_{\text{II}}$  for  $r > R$ . Around the K point of the Brillouin zone the Dirac equation of an antidot or dot has the form

$$H = v_F \vec{\sigma} \cdot \left( \vec{p} + \frac{e}{c} \vec{A} \right) + V(r) \quad (1)$$

with the elementary charge  $e > 0$ , the Fermi velocity  $v_F$ , the Pauli spin matrices  $\vec{\sigma} = (\sigma_x, \sigma_y, \sigma_z)$ , and magnetic vector potential  $\vec{A} = \frac{B}{2}(-y, x, 0)$ . Magnetic field  $\vec{B}$  is along z-axis and is perpendicular to the graphene layer. Since the Hamiltonian commutes with the angular momentum operator  $J_z = -i\partial_\varphi + \sigma_z/2$  the eigenstates can be written in polar coordinates as

$$\Psi_{j,m}(r, \varphi) = e^{i(j-1/2)\varphi} \begin{pmatrix} \chi_A(r) \\ \chi_B(r)e^{i\varphi} \end{pmatrix}. \quad (2)$$

For each angular momentum number  $j = \pm 1/2, \pm 3/2, \pm 5/2, \dots$  there are numerous excited eigenvalues  $E_{j,m}$ , labeled, in increasing order, by  $m = \dots, -2, -1, 0, 1, 2, \dots$  ( $E_{j,m} \geq 0$  for  $m \geq 0$  and  $E_{j,m} < 0$  for  $m < 0$ ).

It follows from Eq.(1) that A and B components of the wavefunction  $\psi_{\sigma,\alpha}$  with energy  $E_a$  satisfy

$$v_F^2 \left[ \left( \vec{p} + \frac{e}{c} \vec{A} \right) \right]^2 \psi_{\sigma,\alpha} = ((E_a - V_\alpha)^2 \mp E_c^2) \psi_{\sigma,\alpha} \quad (3)$$

where the subscript  $\alpha = \text{I, II}$  stands for  $r < R$  or  $r > R$  and the index  $\sigma = -(+)$  denotes for A (B) component. The constants  $E_c = \frac{\hbar v_F}{\ell}$  and  $\ell = \sqrt{\frac{\hbar c}{|B|e}}$  stand for the characteristic energy scale of Dirac electrons in magnetic fields and the magnetic length. If the potential is not piecewise constant another term containing  $\frac{dV}{dr}$  will be present in this equation. The equation has the same mathematical structure as the Schrödinger equation of the two-dimensional Landau levels, but there is an important *difference*: the eigenenergy  $E_a$  and the constant potential  $V_\alpha$  appears together as  $E_{\text{eff}}^2 = (E_a - V_\alpha)^2$ . For  $V(r) = 0$  we obtain the usual result of two-dimensional Dirac electrons in a magnetic field,  $E^2 = 2E_c^2 n$ . Now consider a cylindrical antidot and dot with piecewise constant potentials  $V_a(r)$  and  $V_d(r)$  such that the sum of them is a constant  $V_d(r) + V_a(r) = V$ . Then, it can be shown from Eq.(3) that, when the antidot potential  $V_a(r)$  has an eigenenergy  $E_a$ , the dot potential  $V_d(r)$  will have an eigenenergy  $E_d = V - E_a$  with the *same eigenstate*. Several examples for different pairs of dot and antidot are shown in Fig.1.

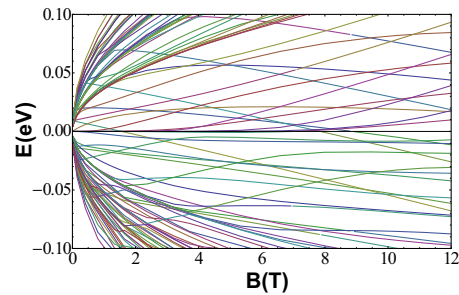


FIG. 2: Energy spectrum of antidot as a function of magnetic field.

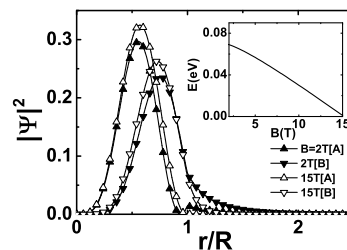


FIG. 3: Plot of the probability wavefunctions of state  $j = 5/2$  at two different value of  $B$ . Inset: its energy level decreases as  $B$  increases.

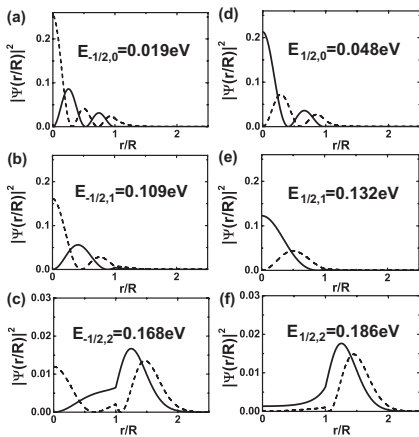


FIG. 4: Probability wavefunctions of antidot with radius  $R$  at  $B = 10.28T$  ( $\ell = 80\text{\AA}$ ), A and B components are represented by solid and dashed lines.

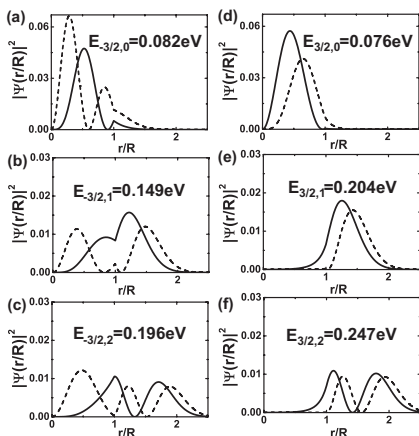


FIG. 5: Same as in Fig.4 but for  $j = \pm 3/2$ .

### III. ANTIDOT EIGENVALUES AND EIGENSTATES

The properties of probability wavefunctions and eigenenergies of a graphene antidot are rather different from those of the ordinary antidot. This is because skipping orbits are not well defined in graphene antidot due to strong Klein tunneling in the presence of a magnetic field. The eigenstates and eigenvalues of the antidot may be found by matching solutions inside and outside of the antidot at the boundary  $r = R$ : the exact eigenstate wavefunctions of Eq.(1) for a cylindrical potential can be described by confluent hypergeometric functions[4, 5] instead of Laguerre polynomials of bulk Landau levels. The energy spectrum is displayed in Fig.2 for  $V_I = 0.26\text{eV}$ ,  $V_{II} = 0$ , and  $R = 200\text{\AA}$ . In the strong magnetic field limit  $R/\ell \rightarrow \infty$  we have tested numerically that the bulk graphene Landau level energies are recovered.

Many positive (negative) energy levels in Fig.2 increase

(decrease) as  $\sqrt{B}$ . Their wavefunctions are localized outside the antidot and are nearly unaffected by the antidot potential. An example is shown in Fig.1(e). Other energy levels display different dependence on  $B$ . Their wavefunctions are affected by the antidot potential and have significant weights on the boundary  $r = R$ . An example is given in Fig.3. As one can expect from the usual Landau level physics, the effective energy  $E_{\text{eff}} = E - V$  of this level increases as  $B$  increases, and its wavefunction becomes more confined in the antidot region. However, this implies that the eigenenergy  $E$  decreases with increasing  $B$ , as shown in the inset of Fig.3.

We have investigated the eigenfunctions for different values of  $E$  and  $j$ . The first three lowest positive energy states for several values of  $j$  are shown in Figs.4 and 5. In contrast to ordinary tunneling physics, we observe a significant penetration into the antidot region: note that for  $j = -1/2$  and  $-3/2$  the probability wavefunctions of A component are smaller than probability wavefunctions of B component in the antidot region. For  $j = 1/2$  and  $3/2$  the opposite is true. The probability wavefunctions of the lowest energy states with  $j = 1/2$  are plotted in Fig.4 (d): in the limit  $r \rightarrow 0$  the wavefunction  $\chi_A(r)$  is proportional to  $e^{-\frac{r^2}{4\ell^2}}$  while  $\chi_B(r)$  is proportional to  $re^{-\frac{r^2}{4\ell^2}}$ . However, for  $j = -1/2$  the opposite is true, as shown in Fig.4 (a):  $\chi_A(r)$  is proportional to  $re^{-\frac{r^2}{4\ell^2}}$  and  $\chi_B(r)$  is proportional to  $e^{-\frac{r^2}{4\ell^2}}$ . We find that as  $|j|$  increases the mean radii of the wavefunctions  $\Psi_{jm}$  increase.

When the mean radius  $\sqrt{\langle r_{jm}^2 \rangle}$  is greater than  $R$  the probability wavefunctions will be peaked in the barrier. In a quantum well the wavefunction for a large  $|j|$ , for example,  $-51/2$ , is thus strongly localized in the *barrier*, as shown schematically in Fig.1(f). This unusual effect is possible because the constant potential of the barrier appears only in  $(E - V)^2$  (see Eq.(3)). The wavefunction of this state has a rather different form in comparison with quasibound states at zero magnetic field with a significant weight inside the dot[2, 10, 12].

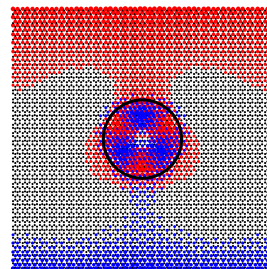


FIG. 6: Occupation probabilities on A and B carbon atoms of a state near the Dirac point with  $E = -0.01\text{eV}$ . Small black dots indicate lattice sites and red (blue) dots indicate values of probability wavefunction on A (B) carbon atoms. The circle represents the antidot. The unit of x and y axis is  $a = 2.46\text{\AA}$ .

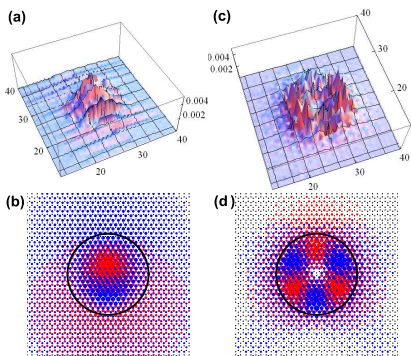


FIG. 7: (a) and (b) display probability wavefunction of a state with  $E = 0.18$  eV and its pseudospin picture, (c) and (d) show probability wavefunction of a state with  $E = -0.04$  eV and its pseudospin picture.

#### IV. ANTIDOT STATES OF ZIGZAG NANORIBBONS

In zigzag nanoribbons it would be interesting to investigate the interplay between Klein tunneling and backscattering[25–27]. We adopt the following model for a nanoribbon with an antidot. The zigzag edges are horizontal along the x-axis and periodic boundary condition is imposed on the left and right edges. The horizontal and vertical lengths of the nanoribbon are  $L_x = 130.35\text{\AA}$  and  $L_y = 130.64\text{\AA}$ . A magnetic field of  $B = 20\text{T}$  is applied perpendicular to the graphene sheet. The radius of the antidot is  $19.68\text{\AA}$  and its the potential height is  $V = 1\text{eV}$ . We solve for eigenstates and eigenvalues in the usual tight-binding Hamiltonian. Fig.6 displays the occupation probabilities on A and B carbon atoms of an eigenstate close to the Dirac point with nearly zero energy (its probability wavefunction is shown in Fig.1(g)). This state is a mixture of zigzag edge and antidot states. Opposite chiralities are found on the opposite sides of the zigzag edges. Since occupation is chiral along the zigzag edges no current flows along the edges. This mixed state is thus not a magnetic edge state. In the absence of an antidot some states near the Dirac point can have long localization lengths while states away from the Dirac point do not[21, 22]. Some of these states with localization lengths comparable to the width of the nanoribbon couple with the antidot, and significant probability wavefunction can be present both at the edges and near the antidot.

On the other hand, probability wavefunctions of eigenstates away from the Dirac point are not peaked along the edges. Their properties are displayed in Fig.7. Figs.7(a) and (b) show an antidot state with the probability wavefunctions that are peaked at the origin of the antidot. Note that a similar feature is observed with Dirac electrons, as shown in Figs.4(a) and (d). In contrast, Figs.7(c) and (d) display a state with the probability wavefunction that is zero at the origin, consistent with

the corresponding result of Dirac electrons, see Figs.5(a) and (d). Tight-binding and Dirac electron models thus yield qualitatively similar results.

#### V. DISCUSSIONS AND CONCLUSIONS

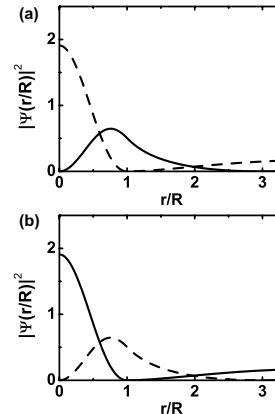


FIG. 8: (a) and (b) display probability wavefunctions of a degenerate pair of K and K' with  $E = 0.188\text{eV}$ . A component is dashed line and B component is solid line, These probability wavefunctions are obtained solving Dirac equations.

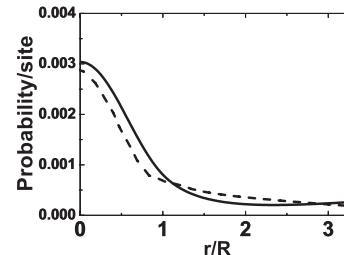


FIG. 9: The solid line shows the total probability wavefunction at lattice sites with  $E = 0.188\text{eV}$  obtained by solving Dirac equation and the dashed line displays the total probability wavefunction with  $E = 0.175\text{eV}$  obtained by solving the tight-binding Hamiltonian.

In our treatment of Dirac equations we ignored the coupling of states of K and K' points due to the presence of a sharp boundary[28] in the antidot potential. In the absence of the sharp boundary states of K and K' points are degenerate with wavefunctions of A and B components exchanged, as shown in Fig.8 (The radius of the antidot is  $19.68\text{\AA}$  and its potential height is  $V = 1\text{eV}$  with the magnetic field  $B = 20\text{T}$ ). The coupling between K and K' points can be included in a tight-binding model, and our calculation shows that this degeneracy of Dirac equations is broken slightly: for example,  $E = 0.188\text{eV}$  splits into  $E = 0.175\text{eV}$  and  $0.181\text{eV}$ , Moreover, the wavefunctions of tight-binding and Dirac equation are rather

close to each other, see Fig.9. Furthermore, inside the antidot A and B components of nearly degenerate tight-binding wavefunctions are approximately similar to those of degenerate solutions of Dirac equations, see Figs.8 and 10: A components are dominant in Figs.8(a) and 10(a) while B components are dominant in Figs.8(b) and 10(b). These tight-binding results demonstrate that the neglect of the coupling between K and K' points in the approach of Dirac equations is a reasonable approximation.

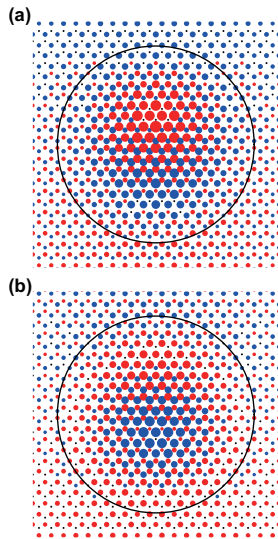


FIG. 10: Occupation probabilities on A and B carbon atoms of a state near the Dirac point with  $E=0.181\text{eV}$ (a),  $E=0.175\text{eV}$ (b). The circle represents the antidot. The unit of x and y axis is  $a = 2.46\text{\AA}$

In this paper we have discussed several unusual properties of tunneling physics of step-like graphene potential barriers in magnetic fields. Scanning tunneling microscope[23] may be used to test strong Klein tunneling effects in antidots since the electron density in the antidot should be non-zero in contrast to an ordinary antidot. Infrared optical transitions[24] may be used to test the symmetry between antidot and dot wavefunctions discussed in this paper: Consider an occupied level  $E_{a,1}$  and an unoccupied level  $E_{a,2}$  in an antidot. Then, according to the proposed symmetry, the absorption transition  $E_{a,1} \rightarrow E_{a,2}$  of the antidot will have the same transition probability as the absorption transition  $E_{d,2} = V - E_{a,2} \rightarrow E_{d,1} = V - E_{a,1}$  of the corresponding dot system. We have also found a significant penetration of wavefunctions deep into the barrier region, as shown in Fig.1(f). This effect is absent in the usual quantum Hall physics in Hall bar geometry, and it may be worthwhile to explore how it may affect quantum Hall edges of graphene.

#### Acknowledgments

This work was supported by the Korea Research Foundation Grant funded by the Korean Government (KRF-2009-0074470). In addition this work was supported by the Second Brain Korea 21 Project.

- 
- [1] Y. Zheng and T. Ando, Phys. Rev. B **65** 245420 (2002).
  - [2] A. Matulis, and F. M. Peeters, Phys. Rev. B **77**, 115423 (2008).
  - [3] P. Hewagegana, and V. Apalkov, Phys. Rev. B **77**, 245426 (2008).
  - [4] S. Schnez, K. Ensslin, M. Sigrist, and T. Ihn, Phys. Rev. B **78**, 195427 (2008).
  - [5] P. Recher, J. Nilsson, G. Burkard, B. Trauzettel, Phys. Rev. B **79**, 085407 (2009).
  - [6] T. Ando, T. Nakanishi, and R. Saito, J. Phys. Soc. Jpn. **67**, 2857 (1998).
  - [7] V.V. Cheianov, and V.I. Fal'ko, Phys. Rev. B **74**, 041403(R) (2006).
  - [8] M.I. Katsnelson, K.S. Novoselov, and A.K. Geim, Nat. Phys. **2**, 620 (2006).
  - [9] N. Stander, B. Huard, and D. Goldhaber-Gordon, Phys. Rev. Lett. **102**, 026807 (2009).
  - [10] P.G. Silvestrov and K.B. Efetov, Phys. Rev. Lett. **98**, 016802 (2007).
  - [11] H.Y. Chen, V. Apalkov, and T. Chakraborty, Phys. Rev. Lett. **98**, 186803 (2007).
  - [12] G. Giavaras, P. A. Maksym, and M. Roy, J.Phys.:Condens. Matter **21**, 102201 (2009).
  - [13] T. G. Pedersen, C. Flindt, J. Pedersen, N. A. Mortensen, A. P. Jauho, and K. Pedersen, Phys. Rev. Lett. **100**, 136804 (2008).
  - [14] M. Vanević, V. M. Stojanović, and M. Kindermann, Phys. Rev. B **80**, 045410 (2009).
  - [15] T. Shen, Y. Q. Wu, M. A. Capano, L. P. Rokhinson, L. W. Engel, and P. D. Ye, Appl. Phys. Lett. **93**, 122102 (2008).
  - [16] J. Eroms, and D. Weiss, New. J. Phys. **11**, 095021 (2009).
  - [17] L. Rosales, M. Pacheco, Z. Barticevic, A. León, A. Latgé, and P. A. Orellana, Phys. Rev. B **80**, 073402 (2009).
  - [18] X. H. Zheng, G. R. Zhang, Z. Zeng, V. M. García-Suárez, and C. J. Lambert, Phys. Rev. B **80**, 075413 (2009).
  - [19] R. Petersen, and T. G. Pedersen, Phys. Rev. B **80**, 113404 (2009).
  - [20] D. Yoshioka, *The Quantum Hall Effect* (Springer, Berlin, 1998).
  - [21] M. Fujita, K. Wakabayashi, K. Nakada, and K. Kusakabe, J. Phys. Soc. Jpn. **65**, 1920 (1996).
  - [22] A. H. Castro Neto, F. Guinea, and N. M. R. Peres, Phys. Rev. B **73**, 205408 (2006).
  - [23] Y.Niimi, H. Kambara, T. Matsui, D. Yoshioka, and H. Fukuyama, Phys. Rev. Lett. **97**, 236804 (2006).
  - [24] Z. Jiang, E. A. Henriksen, L. C. Tung, Y. -J. Wang, M. E. Schwartz, M. Y. Han, P. Kim, and H. L. Stormer,

- Phys. Rev. Lett. **98**, 197403 (2007).
- [25] T. Ando T. Nakanishi, J. Phys. Soc. Jpn. 67, 1704 (1998).
- [26] K. Wakabayashi, Y. Takane, and M. Sigrist, Phys. Rev. Lett. 99, 036601 (2007).
- [27] K. Wakabayashi, Y. Takane, and M. Sigrist, New J. Phys. 11, 095016 (2009).
- [28] A. Rycerz et al., Nature Phys. 3, 172 (2007).